Integrated multi-omics reveals coordinated *Staphylococcus aureus* metabolic, iron transport, and stress responses to human serum

Warasinee Mujchariyakul[1], Calum J. Walsh[1,2], Stefano Giulieri[1,2,3], Cameron Cramond[1], Kim-Anh LêCao[4], Timothy P. Stinear[1,2], Benjamin P. Howden[1,2,5*], Romain Guérillot[1,2*] and Abderrahman Hachani[1,2*]

Affiliations:

[1] Department of Microbiology and Immunology, The University of Melbourne at the Peter Doherty Institute for Infection and Immunity, Melbourne, Victoria, Australia.

[2] Centre for Pathogen Genomics, The University of Melbourne, Melbourne, Victoria, Australia.

[3] Victorian Infectious Diseases Service, Royal Melbourne Hospital, The Peter Doherty Institute for Infection and Immunity, Melbourne, Victoria, Australia

[4] Melbourne Integrative Genomics, School of Mathematics and Statistics, University of Melbourne, Melbourne, Victoria, 3000, Australia.

[5] Microbiological Diagnostic Unit Public Health Laboratory, Department of Microbiology and Immunology, Doherty Institute, University of Melbourne, Melbourne, Victoria, Australia.

* Joint senior authors

Address correspondence to Abderrahman Hachani: abderrahman.hachani@unimelb.edu.au

Keywords: *Staphylococcus aureus*, Multi-omics data integration, Metabolism, iron acquisition, stress responses, bacteremia

Running title: ***Staphylococcus aureus* adaptive responses to human serum**

ABSTRACT

Bloodstream infections caused by *Staphylococcus aureus* remain a leading cause of mortality worldwide. Our understanding of *S. aureus* survival and persistence in human serum, a cell-free fraction of blood hostile for bacteria, is still limited. Here, we applied multivariate data integration methods and network analysis to a multi-omic dataset generated from five clinically prevalent *S. aureus* genotypes exposed to human serum. We observed and then confirmed using isogenic mutants, the significant roles of *gapdhB*, *sucA*, *sirA*, *sstD*, and *perR* in bacterial survival in serum. These data show that metabolic versatility in carbon source usage, iron transport and resistance to oxidative stress are interlinked and central to *S. aureus* fitness in serum, representing potential *S. aureus* vulnerabilities that could be exploited therapeutically.

IMPORTANCE

Bloodstream infections caused by *Staphylococcus aureus* are associated with mortality rates of up to 30%. However, the molecular mechanisms that enable this pathogen to survive in human serum, a nutrient-limited and immunologically hostile environment remain poorly understood. By integrating multi-omic data from five clinically relevant *S. aureus* genotypes and validating key signatures using mutants, we identified conserved genetic determinants critical for bacterial survival in serum. Our findings highlight the interconnected roles of carbohydrate metabolic flexibility, iron acquisition, and oxidative stress resistance in shaping *S. aureus* adaptation to serum. This work advances our understanding of microbial strategies to survive in the bloodstream and demonstrates the potential of multi-omic integration to uncover therapeutic vulnerabilities in bacterial pathogens.

52 **INTRODUCTION**

53 *Staphylococcus aureus* is a significant opportunistic human pathogen (1). As a commensal, *S. aureus*
54 coexists with other members of the human microbiome in up to 30% of the human population,
55 typically colonizing the skin or nares, with the potential to become a lethal pathogen (2). *S. aureus*
56 bloodstream infections are greater than 10 in 100,000 people per year, with the severity of infections
57 compounded by the widespread emergence of resistance to last-line antibiotics such as vancomycin,
58 and mortality rates reaching 20% (3).

59 During bloodstream infections, professional phagocytes and non-cellular immune components,
60 including antimicrobial peptides (AMPs), immunoglobulins and the complement system, target
61 invasive pathogens for clearance (4, 5). While serum does not contain immune cells, it represents a
62 potent bactericidal environment for blood-invasive bacterial pathogens (6-8); an environment against
63 which *S. aureus* has evolved multiple defense mechanisms (1, 9, 10). The bacterium can evade
64 humoral immunity by directly interfering with antibody functions to prevent opsonization for
65 phagocytosis (11, 12), or by degrading complement components (13). *S. aureus* can inactivate AMPs
66 through proteolytic degradation (14), modification of its surface charge, or remodeling both the
67 organization of its cell wall peptidoglycan and the abundance of cardiolipin in its plasma membrane.
68 The latter two processes also contribute to *S. aureus* resistance to cell wall-targeting antibiotics (15).
69 The host can also impose nutritional immunity by sequestering essential nutrients, primarily trace
70 metals like iron, zinc, and manganese to restrict bacterial growth. Bacterial pathogens have evolved
71 mechanisms to circumvent nutritional immunity (16). For example, *S. aureus* has multiple trace
72 metal-sequestering strategies that also contribute to its survival in blood (17).

73 Elucidating the metabolic reprogramming of *S. aureus* in response to serum-derived stressors—such
74 as nutrient limitation and acellular immune factors—can uncover fundamental metabolic pathways
75 that facilitate its adaptation, survival, and persistence in the bloodstream. These insights may inform
76 the development of targeted antimicrobial strategies and rationally designed interventions to mitigate
77 invasive and chronic *S. aureus* infections.

78 We previously reported a comprehensive multi-omics analysis of four clinically significant sepsis-
79 causing bacterial pathogens (*Escherichia coli*, *Klebsiella pneumoniae, S. aureus*, and *Streptococcus*
80 *pyogenes*) following their exposure to human serum (18). This work revealed a set of conserved
81 adaptive responses across these phylogenetically diverse species.
82 Notably, all four pathogens exhibited a coordinated upregulation of lipid metabolic pathways that
83 was associated with extensive remodeling of the cell envelope. This adaptation likely reflects a shared
84 osmoprotective strategy, enhancing bacterial survival in the hostile and nutrient-limited environment
85 of human serum. Building on our multi-omics dataset, this study examines the serum response
86 of *Staphylococcus aureus* across five clinically relevant clonal lineages—BPH2760 (ST1), BPH2819
87 (ST5), BPH2900 (ST22), BPH2947 (ST239), and BPH2986 (ST8). The aim is to identify a conserved
88 set of molecular features that drives species-specific adaptation to serum during septicemia.

89

90 With a focused analysis on *S. aureus*, we refined here our analytical workflow. In our previous study
91 (18), we used a late-integration approach, independently analyzing transcriptomic, proteomic, and
92 metabolomic datasets before mapping significant features to metabolic pathways and Gene Ontology
93 terms. While this revealed broad functional patterns, it lacked the resolution to detect coordinated
94 molecular changes across omics layers or to uncover direct cross-omic relationships. To address these
95 limitations, we adopted the DIABLO framework (Data Integration Analysis for Biomarker discovery
96 using Latent cOmponents) from the mixOmics R package, which applies a sparse, multiblock partial
97 least squares (PLS) method, optimized to integrate all omics datasets within a single multivariate
98 model. By selecting a minimal set of features that co-vary across data types and distinguish between
99 serum- and RPMI-exposed conditions, DIABLO enables the identification of cross-omic interactions,
100 reduces the statistical burden of separate analyses, and preserves the integrated biological context of
101 the *S. aureus* serum response (19, 20). We further interrogated these signatures using differential
102 expression and network-based analyses, and identified interconnected metabolic pathways involved

in serum adaptation through over-representation analysis (ORA) and Gene Set Enrichment Analysis (GSEA).

Our integrated omic analysis shows that *S. aureus* maintains optimal fitness in serum by undergoing changes in key carbohydrate metabolic processes, iron acquisition, and resistance to oxidative stress pathways. This combined response likely enables *S. aureus* to withstand host stressors such as nutritional immunity and promote its survival in human serum.

111 **RESULTS**

112 **Coordinated transcriptomic, proteomic, and metabolomic adaptation of *S. aureus* to serum**

113 We performed multi-omics analysis to find the shared molecular responses to human serum of five
114 *S. aureus* clinical isolates (BPH2760, BPH2819, BPH2900, BPH2947, and BPH2986) (**Figure 1A**).
115 Principal Component Analysis (PCA), a dimensionality reduction method, was applied to each omics
116 layer, revealing clear separation between serum- and RPMI-exposed *S. aureus*. The first principal
117 component (PC1) explained 24%, 22%, 27%, and 29%, respectively, of the total variance in the
118 transcriptomic, proteomic, and metabolomic (GC-MS and LC-MS) datasets, capturing the dominant
119 condition-specific signal (**Figure 1B**). We used DIABLO to integrate the datasets into a unified
120 predictive model of *S. aureus* exposure to human serum. DIABLO is a supervised multiblock method
121 based on sparse Partial Least Squares Discriminant Analysis (sPLS-DA) (19, 20). DIABLO uses the
122 PLS framework to model relationships between molecular features (derived from transcriptomic,
123 proteomic or metabolomic datasets) and phenotypic outcomes. By integrating multiple omics datasets
124 (defined as multiblock) and applying feature selection (sparsity), DIABLO highlights the subset of
125 variables with the greatest discriminatory power – in this case, the staphylococcal molecules most
126 strongly differentiating growth in RPMI versus serum (**Figure 1C-D, Figure S1A-C).** The sample
127 plot showed that the first component captured most of the common serum responses across all five *S.*
128 *aureus* strains, while the second component reflected strain-specific variation (**Figure S1C**). The
129 final DIABLO model used 60 multi-omic features (see methods) that optimally discriminated serum
130 from RPMI exposure on the first component (**Table S1**, **Figure S1D**).

131

132 A coordinated serum response signature was indicated by highly correlated latent components across
133 the omics layers, including transcriptomic, proteomic and metabolomic. The signatures extracted
134 from the omics layers were highly correlated (Pearson's $r > 0.95$) and indicated both class separation
135 and balanced correlation between the datasets (**Figure 1C)**. Loading values from the DIABLO model

136 (**Figure 1D**) show the specific contribution of individual variables, with higher absolute values
137 marking greater discriminative power.
138
139 To explore consistent patterns between omics data, a similarity matrix was calculated across all
140 components and selected features (**Table S1**) and visualized as a network (**Figure 1E)** (21). The
141 network revealed interactions across transcriptomic, proteomic and metabolomic layers, with features
142 grouped by function and showing both positive and negative correlations and suggesting a
143 coordinated response to serum. The staphylococcal pathways enriched among the discriminant and
144 correlated features identified by DIABLO included cell wall biosynthesis, carbohydrate metabolism,
145 iron transport, and defense against host immunity (**Figure 1D, 1E and Table 1)**. CDS and their
146 products central to these pathways exhibited strong positive correlations: i) *glmS*, pivotal in the cell
147 wall biosynthesis and lipid metabolism (via linoleic and oleic acids, and cholesterol metabolites); ii)
148 *gapdhB* and *sucA*, involved in carbohydrate metabolism, and *sstD*, *scdA*, and *isdB*, contributing to
149 iron uptake; and iii) *perR* and *sbi*, supporting oxidative stress resistance mechanisms and immune
150 evasion, respectively. In contrast, genes involved in nucleotide metabolism (*mtaB*, *miaB*, *guaC*) were
151 negatively correlated with carbohydrate metabolism genes (*gapdhB* and s*ucA*) and lipids (linoleic and
152 oleic acids).
153
154 The observed patterns show that *S. aureus* undergoes substantial metabolic adaptation in response to
155 serum, engaging uptake and utilization of serum-derived amino acids, carbohydrates, fatty acids,
156 nucleotides, and their derivatives. Notably, the analysis revealed a marked increase in the abundance
157 of staphylococcal iron acquisition proteins upon serum exposure. In the host environment,
158 extracellular iron is limited and typically sequestered by high-affinity iron-binding proteins such as
159 transferrin, lactoferrin, and hemoglobin within erythrocytes. The elevated levels of both siderophore-
160 dependent (HtsA, SirA, SstA) and siderophore-independent (IsdB) iron acquisition proteins
161 underscore the critical role of iron sequestration in *S. aureus* survival (**Figure 1D**). The integration

of multi-omic data reveals the responses that support metabolic resilience, enabling *S. aureus* to maintain fitness while countering intrinsic serum stressors.

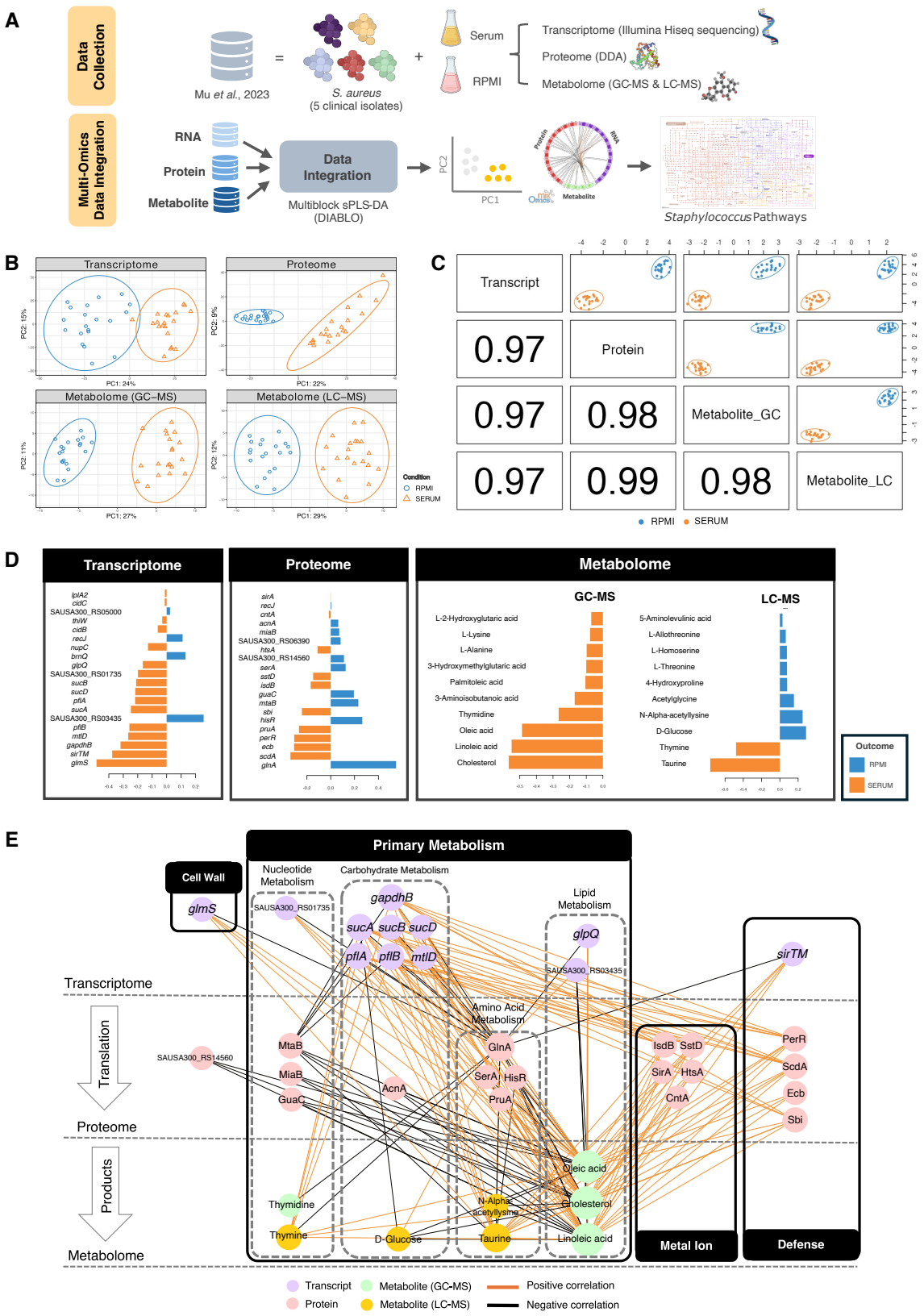

Figure 1. Multi-omics identification of molecular signatures of *S. aureus* adaptation to serum

(A) Schematic workflow of multi-omics analysis to predict *S. aureus* signature molecules in response

167 to human serum; (B) Unsupervised analysis using Principal Component Analysis (PCA). Sample plot
168 from PCA illustrating the consistency of sample clustering across datasets (transcriptomics,
169 proteomics, and metabolomics (GC-MS and LC-MS)), with samples labelled based on media
170 conditions (SERUM and RPMI); (C) Supervised analysis using multiblock sPLS-DA. Diagnostic plot
171 (sample scatter plot), according to media conditions (SERUM and RPMI). The numbers in each block
172 below the diagonal represent correlation coefficients between the first components of each dataset;
173 (D) Loading plot depicting features selected as optimally discriminatory between conditions by PLS-
174 DA from the first component in each dataset; (E) Correlation network visualizing pairwise
175 correlations (> |0.9|) between variables (transcripts, proteins, metabolites). Edge connections
176 represent correlations, with edge colors indicating positive (orange) or negative (black) correlations.
177 Node sizes are proportional to the number of interactions, and node colors represent data types: purple
178 (transcripts), pink (proteins), green (GC-MS metabolites), and yellow (LC-MS metabolites).
179
180 **Table 1.** Functions of selected variables shown in **Figure 1E**

Variable Name	Function	Reference
acnA/ citB (SAUSA300_RS06765)	TCA cycle	(22)
Alpha/beta hydrolase (SAUSA300_RS03435)	Putative lipase/esterase Maintenance of bacterial homeostasis and mediation of host-pathogen interactions	(23, 24)
cntA (SAUSA300_RS13350)	Transport of multiple metals such as nickel, cobalt, zinc, iron, copper, and manganese	(25-27)
ecb (SAUSA300_RS05670)	Complement binding	(28)
gapdhB (SAUSA300_RS08910)	Gluconeogenesis	(29)
glpQ (SAUSA300_RS04655)	Utilization of glycerophosphodiesters (GroPC, GroPI, GroPS, GroPE, and GroPG) and release of glycerol-3-phosphate	(30)
glnA (SAUSA300_RS06485)	Synthesis of L-glutamine from L-glutamate	(31)
guaC (SAUSA300_RS06695)	Conversion of GMP to IMP	(32)
hstA (SAUSA300_RS11760)	Substrate-binding protein in siderophore-dependent iron acquisition pathways	(33)
Hypothetical protein/ hisR (SAUSA300_RS10330)	Repressor in Histidine biosynthesis	(24)
isdB (SAUSA300_RS05535)	Substrate-binding protein in siderophore-independent iron acquisition pathways (heme–iron uptake pathway), interaction with von Willebrand factor, promotion of adherence to endothelial cells	(34, 35)
sbi (SAUSA300_RS13060)	Complement binding	(36)
scdA (SAUSA300_RS01350)	Repair of oxidative and nitrosative damage to iron-sulfur centers and role in cell wall metabolism	(37, 38)
serA (SAUSA300_RS09115)	Biosynthesis of L-serine	(39)
sirA (SAUSA300_RS00605)	Substrate-binding protein in siderophore-dependent iron acquisition pathways	(33)

sirTM (SAUSA300_RS01740)	Regulation of oxidative stress	(40)
sucA (SAUSA300_RS07105)	TCA cycle	(22)
sucB (SAUSA300_RS07100)	TCA cycle	(22)
sucD (SAUSA300_RS06165)	TCA cycle	(22)
sstD (SAUSA300_RS03880)	Substrate-binding protein in siderophore-dependent iron acquisition pathways	(33)
miaB (SAUSA300_RS06405)	Modification of tRNA	(41)
mtaB (SAUSA300_RS08375)	Modification of tRNA	(41)
mtlD (SAUSA300_RS11620)	Conversion of mannitol-1-P to fructose-6-P	(42)
perR (SAUSA300_RS10060)	Sensing of Hydrogen Peroxide (H_2O_2)	(43)
pflA (SAUSA300_RS01160)	Role in Formate metabolism	(44)
pflB (SAUSA300_RS01155)	Role in Formate metabolism and promotion of biofilm persistence	(44, 45)
Polyisoprenoid-binding protein (SAUSA300_RS14560)	Role in the electron transport system	(32, 46)
Protein-ADP-ribose hydrolase (SAUSA300_RS01735)	Reversal of ADP-ribosylation in posttranslational modification	(47)
pruA/rocA (SAUSA300_RS13840)	Catabolism of proline to glutamate	(48)

Network and enrichment analyses reveal *S. aureus* shared and strain-specific responses to serum

Differentially expressed (DE) genes or proteins for each strain were identified and further subjected to an intersection analysis. This analysis showed that at the transcript level, 143 genes were up-regulated, and 65 genes were down-regulated in response to serum. At the proteomic level, there were 21 up-regulated and 17 down-regulated proteins in response to serum (**Figure S2A-B, Table S2**). We performed a Pathway Enrichment Analysis (PEA), including an overrepresentation analysis (ORA) and a gene set enrichment analysis (GSEA), to reduce the complexity of data and find overrepresented pathways elicited upon exposure to serum. ORA is widely used to identify over-represented biological functions in DE gene sets, performing best when handling wide gene expression differences. Genes were filtered using criteria of log2 fold change (log2FC) > 1 and adj-P value < 0.05. To improve the granularity of PEA outputs, a GSEA analysis was also applied to capture pathways where gene expression changes were more subtle but consistently enriched, enabling the

196 detection of significant, but lower-magnitude responses. Using the similarity in gene subsets shared
197 between pathways, we also conducted a network analysis to find interactions among the enriched
198 pathways across the omics layers (**Figure 2A, Figure S3A-J, Table S3**). Consistent with previous
199 DIABLO findings, ORA and GSEA identified four distinct functional modules comprising
200 carbohydrate metabolism, ribosome-associated pathways, iron acquisition, and nucleotide
201 metabolism (**Figure 2B-E**).
202
203 The carbohydrate metabolism module was composed of the glycolysis/gluconeogenesis pathway,
204 along with other carbohydrate-processing routes such as phosphotransferase systems (PTS) (**Figure**
205 **2B-C**). Upregulated carbohydrate transporter genes, *uhpT*, *mtlA*, *fruA*, *glcC*, *lacE*,
206 SAUSA300_RS01760, and *rbsU,* support the usage of various saccharides, including glucose,
207 fructose, lactose, D-mannitol, and ribose (**Table S2**). Once transported and phosphorylated by PTS,
208 carbohydrates such as glucose and fructose, are processed by glycolysis and converted into ribose-5-
209 phosphate, glyceraldehyde-3-phosphate, and fructose-6-phosphate intermediates. These key
210 metabolites bridge glycolysis to nucleotide and lipid metabolism (49, 50) (further detailed in **Figure**
211 **4)**, thereby enhancing the staphylococcal metabolic flexibility in serum. In contrast to other metabolic
212 modules, our network analysis revealed that ribosome-associated pathways were largely isolated,
213 exhibiting no direct connectivity with broader metabolic networks (**Figure 2C, Figure S3A-D**).
214 Transcriptome profiling indicated a suppression of ribosome biogenesis following serum exposure,
215 characterized by the downregulation of genes encoding 30S and 50S ribosomal subunit proteins
216 (**Table S2 and S3)**. Expression of the translational GTPase *typA* (also known as *bipA*), an important
217 regulator of ribosome assembly and translational fidelity under stress conditions (51, 52), was also
218 significantly reduced (**Table S2)**. These findings show that the protein biogenesis is downregulated
219 as part of a stress-adaptive response of *S. aureus* to serum.
220

221 Among the proteomic changes induced by serum exposure, iron acquisition and nucleotide
222 metabolism pathways showed the most substantial alterations (**Figure S1C**). Notably, there was a
223 marked increase in the abundance of iron transport proteins, including SirA, FhuC, SstC, SstD, HtsA,
224 IsdB, IsdE, and IsdI. In addition, elevated levels of ScdA and CntA (53) -proteins involved in iron-
225 sulfur cluster binding - alongside the downregulation of *miaB* (54), suggest the activation of iron-
226 sparing strategies by *S. aureus* under serum conditions (**Tables S2** and **S3**). The significant increase
227 in levels of ScdA and CntA, iron cluster binding proteins, concomitant with the downregulation of
228 *miaB*, point to the engagement of staphylococcal iron-sparing strategies during serum exposure
229 (**Table S2** and **S3**). Thus, *S. aureus* coordinates enhanced iron uptake with the regulation of iron
230 incorporation into metalloproteins to efficiently manage iron availability during serum exposure
231 (**Figure 2D**, **Figure S1B** and **S3F**).
232
233 Proteins involved in nucleotide metabolism, particularly those associated with the inosine
234 monophosphate (IMP) biosynthetic pathway, were prominently increased across all *S. aureus* isolates
235 (**Figure 2E** and **Figure S3H**). This pathway is central to the synthesis of purine nucleotides such as
236 adenosine monophosphate (AMP) and guanosine monophosphate (GMP), critical molecules for DNA
237 replication, RNA transcription, and cellular proliferation. These shifts underscore the prioritization
238 of iron homeostasis and nucleotide biosynthesis as key adaptive strategies employed by *S. aureus* to
239 support survival and growth in serum.
240

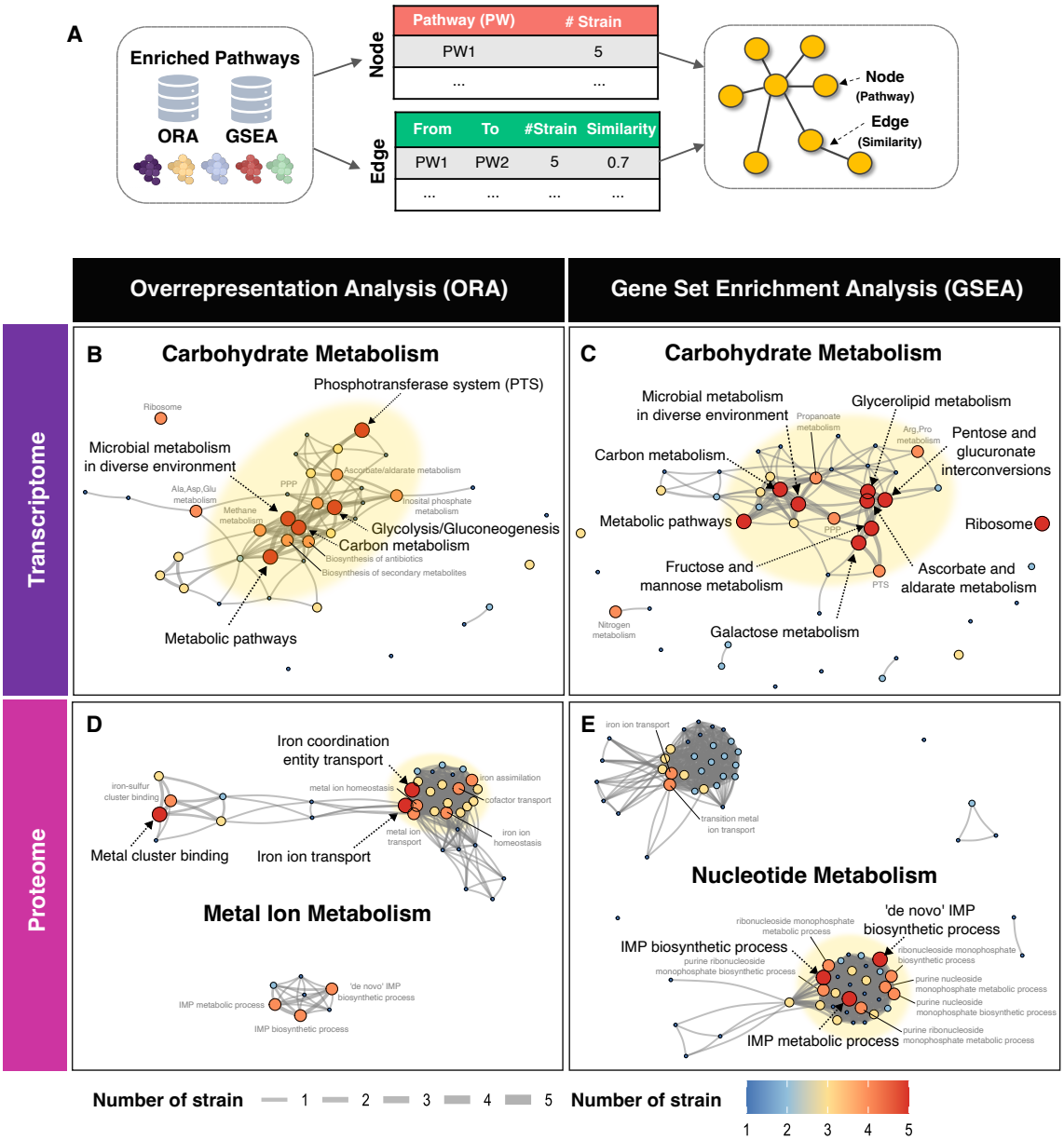

241

242

243 **Figure 2. Clustering of transcriptomics and proteomics data into function-related modules**

244 (A) Workflow overview for network analysis of enriched pathways identified from over-
245 representation analysis (ORA) and gene set enrichment analysis (GSEA), with nodes representing
246 pathways and edges representing pairwise similarity (Sim) between enriched terms or pathways
247 (PW), calculated using Jaccard's similarity coefficient. (B-C) ORA and GSEA of transcriptomic data.
248 (D-E) ORA and GSEA of proteomic data. Dot sizes and colors represent the number of strains sharing
249 the same enriched pathways. Edge widths indicate the number of strains with interactions between

250 pathways, while edge lengths reflect pathway similarity. Yellow shading highlights denote
251 functionally related modules.
252

253 **Experimental validation of predicted molecular signatures of *S. aureus* responses to human**
254 **serum**

255 To confirm findings from the multi-omic integration and pathway enrichment analyses, we assessed
256 the fitness of *S. aureus* transposon mutants in genes involved in carbon metabolism, iron acquisition,
257 and oxidative stress resistance, relative to their parental wild-type USA300 JE2 strain, in the presence
258 of serum (**Figures 1E and 3A**). We initially verified the genetic relatedness of the five *S. aureus*
259 bloodstream isolates to the laboratory strain JE2, used for this phenotypic validation. We observed a
260 high conservation of the *S. aureus* core genome (2,222 core genes- representing 71% of JE2 genome-
261 and 903 accessory genes). Strain JE2 was most closely related to the clinical isolate BPH2986, with
262 both belonging to the ST8 USA300 lineage and differing by only 73 single nucleotide polymorphisms
263 (SNPs) (**Figure S4A-D**).

264 The DIABLO integrative model identified *gapdhB* and *sucA* as key contributors to response to
265 serum, exhibiting the highest loading values (**Figure 1D, Table S1)**. Disruption of either gene
266 resulted in a significant reduction in bacterial fitness in serum, showing they both play important roles
267 in response to serum exposure (**Figure 3B and S5A**).

268 GapdhB, a gluconeogenic enzyme, and SucA, an enzyme of the tricarboxylic acid (TCA) cycle,
269 represent distinct nodes in the carbon metabolism pathway. This functional difference suggests that
270 their contributions to *S. aureus* fitness may be contingent upon the availability and type of carbon
271 substrates. To test this, we compared the growth and respiration phenotypes of
272 *gapdhB* and *sucA* transposons mutants with a 190 different carbon sources (Biolog Inc., Hayward,
273 CA, USA), to that of the wild type *S. aureus* JE2 strain. These carbon sources fell into several broad
274 categories, including carbohydrates (mono-, di-, and oligosaccharides), carboxylic acids (short-chain

275 fatty acids like acetate, dicarboxylic acids like fumarate, and hydroxy acids like lactate), amino acids,
276 alcohols, nucleosides and other organic compounds. The metabolic activities of *S. aureus* JE2 wild
277 type (WT), *gapdhB* and *sucA* transposon mutants were more strongly influenced by individual carbon
278 sources, thus compound-specific, than by their broader carbon classification (**Figure S6A**).

279

280 Among the tested carbon sources, the carboxylic acid methyl pyruvate, α-D-glucose, D-glucosamine,
281 and other hexoses, significantly enhanced respiration in both WT and mutants, whereas glyoxylic
282 acid and itaconic acid suppressed respiration (**Figure 3C, Figure S6** and **Table S4**). Notably, methyl
283 pyruvate supplementation partially rescued the respiratory deficiency of the *sucA* mutant, surpassing
284 WT levels, while it failed to restore *gapdhB* mutant activity to WT levels (**Figures 3C and S6B**).
285 Whilst we showed that the metabolic responses of WT and mutant strains were shaped more by
286 specific carbon compounds rather than by their general category, supplementation with methyl
287 pyruvate revealed distinct roles for *gapdhB* and *sucA* in pyruvate catabolism (**Figure S6B**). Methyl
288 pyruvate, a membrane permeable pyruvate analog, enter cells where it is converted to acetyl-coA. In
289 the absence of *sucA,* supplementation with methyl pyruvate provides an alternative carbon source that
290 bypasses the glycolytic block caused by the absence of conversion of 2-oxaloglutarate to succinyl-
291 coA in the TCA cycle. GapdhB catalyzes the conversion of glyceraldehyde-3-phosphate (G3P) to
292 1,3-biphosphoglycerate in the gluconeogenic direction (29). In a *gapdhB* mutant, the gluconeogenic
293 pathway is blocked, so cells cannot convert methyl pyruvate (see primary metabolism in **Figure 4**).
294

295 To investigate the contribution of iron acquisition systems to *Staphylococcus aureus* fitness in serum,
296 we evaluated four mutants, with transposon insertions disrupting genes *htsA*, *sirA*, *sstD*, and *isdB*.
297 The *htsA* and *sirA* genes encode substrate-binding proteins associated with the siderophores
298 staphyloferrin A (SA) and staphyloferrin B (SB), respectively, both of which facilitate iron extraction
299 from transferrin in serum (33). The gene *sstD* encodes a component of the Sst system, which mediates

300 iron uptake from host-derived catechols (33). In contrast, *isdB* encodes a cell wall-anchored
301 hemoglobin receptor within the Isd (iron-regulated surface determinant) system, a siderophore-
302 independent pathway that enables heme iron acquisition (**Figure 3D**). Proteomics revealed
303 significantly elevated levels of HtsA, SirA, SstD, and IsdB following serum exposure, indicating their
304 upregulation in response to iron-limited conditions (**Figure S1C**). *S. aureus sirA* and *sstD* transposon
305 mutants had significantly impaired fitness in serum, consistent with the importance of SB-mediated
306 and catechol-mediated iron uptake under these conditions (**Figure 3E**). In contrast, disruption
307 of *htsA* did not significantly affect fitness, aligned with previous findings that SB biosynthesis, unlike
308 SA, is independent of TCA cycle activity and may be preferentially utilized in iron-restricted
309 environments (55). The reduced fitness observed in the *sirA* mutant likely reflects the impaired
310 utilization of SB as an iron capture process in serum.

311 Interestingly, the *isdB* mutant exhibited no fitness defect in commercially sourced serum, likely due
312 to the absence of hemoglobin or heme (56), which are typically sequestered within red blood cells
313 and thus unlikely present in commercial cell-free serum preparations. These findings underscore the
314 context-dependent utilization of iron acquisition systems in *S. aureus* and highlight the critical role
315 of siderophore- and catechol-mediated pathways in supporting staphylococcal survival in iron-limited
316 host environments.
317

318 Oxidative stress constitutes a fundamental component of the host immune response, primarily through
319 the generation of reactive oxygen species (ROS) aimed at neutralizing invading pathogens. To
320 counteract ROS, bacteria have evolved intricate oxidative stress response mechanisms (57, 58).
321 Central to these systems are redox-sensitive transcriptional regulators such as OhrR, OxyR, and PerR,
322 which enable the detection of specific ROS and orchestrate the staphylococcal defensive gene
323 expression programs (59). In *S. aureus*, PerR functions as a principal peroxide sensor and belongs to
324 the ferric uptake regulator (Fur) family of metalloregulatory proteins, which includes Fur and Zur
325 (60). These regulators require metal cofactors for activity, underscoring the metal-dependent nature

326 of oxidative stress sensing. In our analysis, PerR emerged as a key molecular determinant of oxidative
327 stress resistance in *S. aureus*, a finding confirmed by experimental testing. The *per* mutant exhibited
328 a significant fitness defect in serum supplemented with 0.25- and 0.5 mM hydrogen peroxide (H_2O_2),
329 with the most pronounced impairment observed after 20 hours of exposure to 0.5 mM H_2O_2 (**Figure**
330 **3F, Figure S5D**). Also, exposure to serum elicited significant production of staphyloxanthin, encoded
331 by the *crt* operon, and whose production is under the control of PerR (**Figure 3G, Figure S5E**). These
332 results underscore the critical role of PerR in facilitating *S. aureus* survival under oxidative stress
333 conditions, as encountered by *S. aureus* in serum, highlighting its importance in maintaining bacterial
334 fitness in ROS-rich host environments.

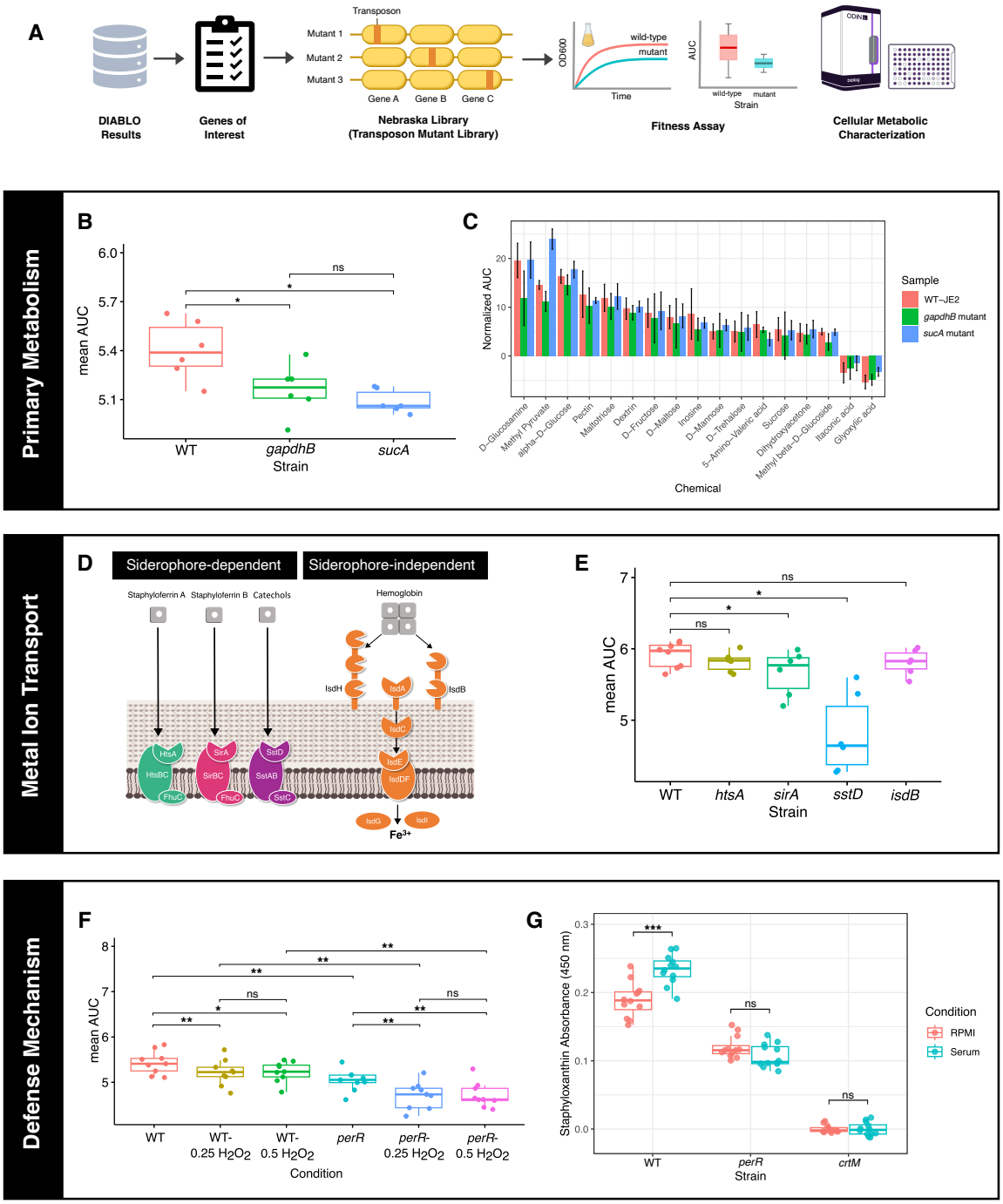

Figure 3. Phenotypic validation of molecular signatures of serum adaptation and metabolic characterization

(A) Workflow of phenotypic validation experiments to confirm the predicted molecular signatures of *S. aureus* exposed to human serum. (B) Box plots comparing Area-under-the-curve (AUC) values of *gapdhB* and *sucA* mutants to wild-type *S. aureus* (WT-JE2) grown in presence of serum, for 20 hours (n = 6 biological replicates). (C) Fitness profiling of *S. aureus* represented by the rate of bacterial respiration in presence of different carbon sources (corresponding to metabolic activity inferred from

343 the reduction of tetrazolium). Plots comparing Area-under-the-curve (AUC) values of *gapdhB* and
344 *sucA* mutants to wild-type *S. aureus* (WT-JE2) grown in presence of sole carbon sources, for 24 hours
345 (n = 3 biological replicates). (D) Representation of iron acquisition pathways in *S. aureus.* (E) Box
346 plots comparing AUC values of iron transport-deficient mutants (*htsA, sirA, sstD, isdB*) to WT-JE2
347 cultured in serum for 20 hours (n = 6 biological replicates). (F) Box plots comparing AUC values of
348 *perR* mutant to WT-JE2 grown in serum with different concentrations of H_2O_2 for 20 hours (n = 9
349 biological replicates), demonstrating the role of *perR* in oxidative stress resistance. (G) Quantification
350 of Staphyloxanthin production by WT-JE2, *perR* and *crtM* mutants, following 5 h incubation in RPMI
351 or serum (n = 12 replicates, generated from 4 different cultures using 2 serum batches). All data points
352 represent mean values for at least three independent biological replicates, with error bars indicating
353 the corresponding standard deviations from the means.
354 Statistical significance between WT-JE2 and isogenic mutants was determined using the **Wilcoxon**
355 **paired test**. Significance levels are indicated by asterisks: *$p < 0.05$, **$p < 0.01$, and ***$p < 0.001$.
356

357 **Integrated metabolic responses of *S. aureus* to human serum**

358 To conceptualize the dynamic remodeling of *S. aureus* metabolism in response to serum, we
359 constructed a scaffolded metabolic network based on curated literature (61-74). This network was
360 overlaid with the significant changes in key enzymes identified through single omics analysis (genes
361 upregulated in orange, downregulated in light blue) and by DIABLO integration (genes and
362 metabolites in red), combined with network analyses (**Figure 4, Tables S2–S5**). This integrative
363 approach revealed that *S. aureus* mounts a broad and adaptable metabolic response to the challenges
364 posed by the serum environment, particularly in the utilization of diverse carbon sources including
365 carbohydrates, amino acids, and lipids. Multi-omics data (**Figure S7A–D**) highlighted consistent
366 upregulation of gluconeogenic and TCA cycle enzymes at both transcript and protein levels,
367 indicating a metabolic shift toward energy-efficient carbon utilization upon exposure to serum.
368

369 Carbohydrate metabolism was organized around three key metabolic nodes—glucose-6-
370 phosphate/fructose-6-phosphate (G6P/F6P), glyceraldehyde-3-phosphate/dihydroxyacetone
371 phosphate (GA3P/DHAP), and pyruvate (**Figure 4**, purple nodes embedded in
372 glycolysis/gluconeogenesis)—which serve as convergence points for nutrient assimilation. The
373 upregulation of carbohydrate transporter genes (*uhpT, mtlA, fruA, glcC, lacE, SAUSA300_RS01760,*
374 *rbsU*) in serum aligns with our findings that saccharides, including the hexose monosaccharides α-
375 D-glucose, D-fructose, D-mannose and disaccharides D-maltose, and sucrose, significantly enhanced
376 the metabolic activity of *S. aureus* (**Figures 3C and S6A**). Notably, saccharides such as G6P,
377 fructose, and mannose, but not glucose, have been shown to influence virulence gene expression (75).
378 Our transcriptomic data support this, revealing increased expression of γ-hemolysins genes (*hlgA,*
379 *hlgB, hlgC*) and immune evasion genes (*ecb, sbi, vraX*) across five *S. aureus* strains in serum. In
380 particular strain BPH2986 (ST8) exhibited strong upregulation of *lukF-PV* and *lukS-PV* genes,
381 encoding Panton-Valentine leucocidins (**Figure S8A**). These findings suggest that carbohydrates,
382 such as fructose and mannose, present in serum, support the metabolic activity of *S. aureus* while
383 increasing virulence gene expression, in contrast to the glucose-rich RPMI.
384
385 Amino acids and peptides from serum further contribute to the metabolic adaptability of *S. aureus* by
386 entering carbohydrate metabolism and the TCA cycle through key intermediates such as pyruvate, 2-
387 oxoglutarate, and oxaloacetate. These entry points define three functional groups of amino acids: (1)
388 pyruvate-yielding, (2) 2-oxoglutarate-yielding, and (3) oxaloacetate-yielding (**Figure 4**). Our
389 transcriptomic data revealed significant upregulation of enzymes involved in amino acid catabolism,
390 including *pckA* (encoding pyruvate carboxykinase) and *gudB* (encoding glutamate dehydrogenase),
391 consistent with elevated intracellular levels of phosphoenolpyruvate (PEP) and 2-oxoglutarate
392 (**Figure S7C–E**). Genes encoding enzymes for the degradation of glutamate (*gudB*), proline
393 (*pruA/rocA*, *putA*), arginine (*rocD/argD*), and histidine (*hutI, hutG*) were also upregulated, indicating
394 preferential catabolism of these amino acids during serum exposure. These findings are consistent

395 with previous reports identifying glutamate and its precursors as major carbon sources supporting *S.*
396 *aureus* proliferation (65), positioning glutamate as a central amino acid in the adaptive response to
397 serum.
398
399 Exposure to human serum triggered a marked upregulation of *S. aureus* genes involved in lipid and
400 phospholipid degradation, including *glpQ* and *gehA*. This suggests an enhanced capacity in using
401 host-derived lipids—such as cholesterol, linoleic acid (C18:2), and oleic acid (C18:1)—as nutrient
402 sources. These lipids are metabolized into glycerol-3-phosphate (G3P), which can be then funneled
403 into the carbohydrate metabolism via the GA3P/DHAP node. Interestingly, our transcriptomic data
404 revealed downregulation of *tpiA*, which encodes triosephosphate isomerase, an enzyme responsible
405 for the reversible interconversion of GA3P and DHAP. This suggests a potential bottleneck at this
406 metabolic junction, which may constrain glycolytic flux and influence the efficiency of carbon
407 utilization from lipids present in serum.
408
409 Counteracting innate immune defences is essential for *S. aureus* survival during bloodstream
410 infection. Upon exposure to human serum, *S. aureus* exhibited robust transcriptional upregulation of
411 a broad range of virulence-associated genes involved in immune evasion, host colonization, and
412 pathogenesis. These include genes encoding complement-evasion proteins (*ecb, sbi, vraX*), pore-
413 forming cytotoxins (*hlgA, hlgB, hlgC*), superantigen-like proteins (*ssl13, ssl14*), and the fibrinogen-
414 binding adhesin *clfA*. This coordinated immune evasion strategy underscores the pathogen's capacity
415 to rapidly adapt to immune pressures and enhance its invasive potential in the bloodstream.
416
417 Serum exposure also elicited a pronounced oxidative stress response in *S. aureus*. DIABLO analysis
418 identified *perR,* which encodes the peroxide-sensing transcriptional regulator PerR, as a key
419 molecular signature of staphylococcal adaptation to serum. Consistent with this, genes involved in
420 carotenoid biosynthesis —*crtM, crtN, crtQ* —were upregulated, suggesting enhanced anti-oxidative

421 defence through increased production of staphyloxanthin, a carotenoid pigment known to protect
422 against reactive oxygen species (76). In parallel, elevated expression of *scdA*, a gene involved in iron-
423 sulfur cluster repair, indicates activation of protein maintenance pathways essential for preserving
424 enzymatic and cellular functions under oxidative stress (37, 77).
425
426 Our integrative approach has highlighted the high adaptive capacity of *S. aureus* to withstand human
427 serum exposure. Through the coordinated activation of nutrient acquisition systems, oxidative stress
428 defenses, and virulence-associated mechanisms, *S. aureus* enhances its ability to survive and persist
429 during systemic infection.
430

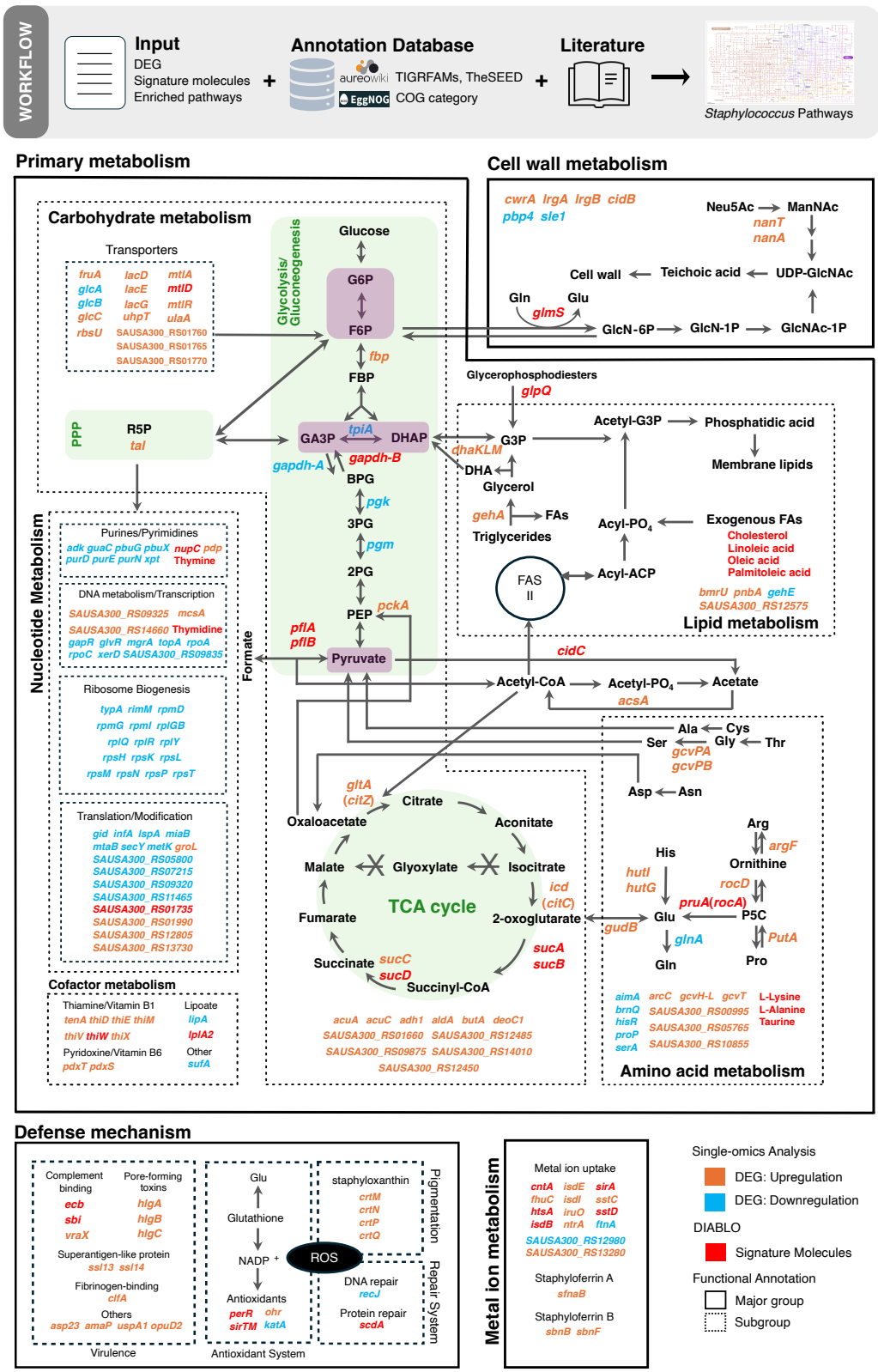

Figure 4. Integrated metabolic and virulence adaptation of *S. aureus* in response to serum

Systems-level metabolic reprogramming of *S. aureus* upon exposure to serum, integrating single- and multi-omics data. The depicted key metabolic pathways include glycolysis/gluconeogenesis (upright rectangle shaded in light green), the pentose phosphate pathway (PPP), the tricarboxylic acid (TCA)

436 cycle (circle shaded in light green), nucleotide biosynthesis, ribosome biogenesis, thiamine (vitamin
437 B1) biosynthesis and transport, cell wall biosynthesis, and lipid metabolism. Host-responsive
438 processes such as immune evasion, metal ion acquisition, and oxidative stress responses are also
439 represented. The name of enzyme is colored to indicate changes in gene expression following serum
440 exposure identified by single omics (compared to RPMI), with orange: increased expression, light
441 blue: decreased expression. Variables predicted by DIABLO (multi-omics analysis) are in red,
442 indicating their status as signature molecules of *S. aureus* serum response.

443

444 **Discussion**

445 Whilst a leading cause of lethal bacteremia, *S. aureus* must contend with the nutrient-limited and
446 immunologically hostile conditions of the bloodstream to establish infection and cause disease. In the
447 bloodstream, the bacterium uses a large panoply of virulence factors to evade clearance by cellular
448 and humoral immunity (1, 78, 79). Notwithstanding bactericidal immune cells patrolling the
449 bloodstream, serum remains a challenging environment for *S. aureus* due to the paucity of free forms
450 of essential nutrients, often complexed to large proteins (e.g. iron ions complexed to transferrin) (80).
451 Several studies have shown that *S. aureus* has evolved multiple mechanisms, unrelated to its
452 cytotoxicity, to overcome the nutritional constrains and acellular insults of the serum (16). While
453 informing on discrete *S. aureus* nutritional stress responses, these mechanisms were studied in
454 isolation and did not consider the concomitant adaptive responses to the serum environment. Building
455 on our previous work showing that four diverse blood-invasive pathogens, including *S. aureus*,
456 remodeled their cell wall to adapt to serum (18), we used a multi-omics approach to define the shared
457 serum-adaptive response of *S. aureus* across five clinical isolates. Such approach offers a systems-
458 level view of microbial adaptation in response to environmental stimuli, by linking molecular changes
459 across genomic, transcriptomic, proteomic, and metabolomic layers (81-83). Using integrative
460 machine learning-based multivariate analyses, differential expression profiling, and network-based

461 approaches, our study identified staphylococcal reprogramming in cell wall biosynthesis, carbon
462 metabolism, iron transport, and defense mechanisms in response to serum.
463
464 The experimental validation of the dominant outputs identified by our integrative framework
465 confirmed the importance of *gapdhB*, *sucA*, *sirA*, *sstD*, and *perR* genes for staphylococcal fitness in
466 serum (**Figure 3**). These results align with the positive co-variation patterns observed in the DIABLO
467 model, suggesting a functional interdependence among the pathways involving these genes (**Figure**
468 **1C**). Whilst critical for optimal fitness in serum, *gapdhB* and *sucA* have distinct functions in carbon
469 metabolism. Metabolic profiling revealed that hexose saccharides (e.g., α-D-glucose, D-glucosamine)
470 enhanced the metabolic activity in WT and *gapdhB* and *sucA* mutants, through glycolysis,
471 gluconeogenesis, PPP, and TCA cycle. While methyl pyruvate partially restored bacterial respiration
472 in the *sucA* mutant, likely via conversion to acetyl-CoA and oxaloacetate (84), the *gapdhB* mutant
473 remained metabolically impaired, reflecting incomplete gluconeogenesis and insufficient PPP
474 intermediate generation (**Figures 3B** and **S6**). While highlighting the importance of gluconeogenesis
475 for *S. aureus* during serum exposure, these results further underscore the non-redundant roles of
476 GAPDH homologs (*gapdhA*, *gapdhB*) in maintaining metabolic flux (29). Interestingly, pyruvate was
477 shown to activate *S. aureus* regulatory networks controlling the production of leucocidins, and thus,
478 potentiating the cytotoxicity of *S. aureus* (85). Conversely, exposure to glyoxylate and itaconate
479 inhibited *S. aureus* metabolism **(Figures 3C** and **S6)**. The bacterium does not use the glyoxylate shunt
480 (86), rendering glyoxylate toxic due to metabolic imbalance. Moreover, glyoxylate is limited in
481 serum, as humans lack an active glyoxylate cycle (65). Itaconate, an immunometabolite produced by
482 macrophages, further exacerbates stress by directly inhibiting glycolysis (86, 87). These findings
483 highlight the potential of *S. aureus* metabolic vulnerabilities that could be exploited therapeutically,
484 such as inhibitors of the bacterial glycolysis and the TCA cycle (88). However itaconate was shown
485 to increase tolerance to aminoglycosides, limiting its potential as adjunct therapeutic (89). We
486 constructed a metabolic map of *S. aureus* that integrates the predicted signature molecules

487 elicited/repressed in serum (**Figure 4, Table S4**). This illustrates the flexibility of *S. aureus* in using
488 diverse carbon sources in serum, such as hexose saccharides, amino acids yielding 2-oxoglutarate
489 (e.g., Glu, Pro, Arg, His), and host lipids and fatty acids (e.g., cholesterol, linoleic acid (C18:2), and
490 oleic acid (C18:1)) to support its survival. Hexose saccharides have also been shown to regulate
491 virulence gene expression (75). Peptides and amino acids present in serum contribute to *S. aureus*
492 metabolism by entering glycolysis via pyruvate or intermediates of the TCA cycle (e.g., 2-
493 oxoglutarate, oxaloacetate). Transcriptomic analysis revealed significant upregulation of key
494 enzymes involved in amino acid catabolism, including pyruvate carboxykinase (*pckA*) and glutamate
495 dehydrogenase (*gudB*), phosphoenolpyruvate (PEP) and 2-oxoglutarate (**Figure S7C-E**). Notably,
496 we found a significant increase in gene expression of enzymes (e.g. *gudB*, *pruA* [*rocA*], *putA, rocD*
497 *[argD], hutI,* and *hutG*) converting amino acids (e.g., Glu, Pro, Arg, His) to 2-oxoglutarate in amino
498 acid catabolism, indicating the usage of these amino acids by the bacteria in serum. This is consistent
499 with the observation that glutamate, and the amino acids that can be converted into glutamate (Pro,
500 Arg, and His), provide most of the carbon required for bacterial growth (65). Several upregulated
501 metabolic pathways facilitating glutamate production, driven by *pruA* (converting proline to
502 glutamate) and *putA* (proline dehydrogenase) underscore glutamate as a key intermediate metabolite
503 in the adaptive response of *S. aureus* to serum. Concurrently, the downregulation of glutamine
504 synthesis, through decreased expression of *glnA*, suggests a reduction in the utilization of glutamate.
505 Excess levels of glutamate did not significantly influence the respiration or growth of JE2 WT (**Table**
506 **S4**), although several studies have highlighted the important role of glutamate in protecting bacteria
507 from cell death under stress (90-93).
508
509 Iron is an important determinant for *S. aureus* fitness (80). Our analyses confirmed the role of multiple
510 iron acquisition mechanisms in iron-limited host environments such as serum. Interestingly, mutants
511 lacking *htsA* and *isdB*, both involved in iron acquisition, displayed growth rates comparable to that
512 of JE2 WT, suggesting some iron uptake system redundancy (**Figure 3E**). This observation is

513 consistent with prior research reporting the upregulation of iron acquisition systems such as Isd and
514 SirABC in *S. aureus* cultured in serum or blood (94). Further studies are necessary to understand the
515 specificity of iron-acquisition modules in iron-limited environments in the context of bacterial
516 metabolic reprograming during bloodstream infection.
517
518 Resistance to oxidative stress in serum was also highlighted by our analyses and confirmed
519 experimentally. Staphyloxanthin is a carotenoid pigment produced by *S. aureus* that enhances
520 resistance to oxidative stress. The biosynthesis of staphyloxanthin is encoded by the *crtOPQMN*
521 operon, primarily activated by σB, and its expression is influenced by redox-responsive regulators.
522 PerR, a peroxide-sensing transcriptional repressor identified by DIABLO as a response signature to
523 serum, plays a pivotal role by controlling genes that detoxify reactive oxygen species, such as *katA*
524 that encodes for the catalase. Loss of PerR function disrupts oxidative stress homeostasis, which can
525 alter σB activity, leading to reduced production of staphyloxanthin (**Figure 3G and Figure S5E**).
526 Thus, our data confirmed PerR is a key player linking peroxide sensing to virulence factor regulation
527 upon serum exposure (76).
528
529 Serum exposure also engaged *S. aureus* defense mechanisms against acellular immunity. We
530 observed upregulation of virulence-related genes including complement-binding proteins (e.g., *ecb*,
531 *sbi*, *vraX*) (28, 95, 96), pore-forming toxins (e.g., the γ-hemolysins *hlgA*, *hlgB*, *hlgC*) (97),
532 superantigen-like proteins (*ssl13*, *ssl14*) (98), and the fibrinogen-binding protein *clfA* (99) (**Figures**
533 **4 and S8)**. Such responses would prime *S. aureus* against clearance by immune cells. Mechanisms
534 for evasion from host antibodies and the complement system were also engaged, including the
535 immunoglobulin-binding protein (Sbi) and complement convertase inhibitor (Ecb) (28, 100). *S.*
536 *aureus* sensing and responses to host oxidative stress were also identified as important for serum
537 exposure survival (40, 43, 47, 60). Future studies examining how serum promotes *S. aureus* biofilm

538 formation on host-like surfaces could provide deeper insight into the roles of ClfA, Ecb and other
539 adherence factors during bloodstream infections.
540

541 **Conclusion and perspectives**

542 This study exploited multi-omics analyses, including machine learning-based approaches, DE
543 analysis and network analysis, to uncover the major *S. aureus* features engaged in response to human
544 serum. Our findings highlight the parallel activation of nutrient acquisition systems, oxidative stress
545 defenses, and virulence-associated mechanisms, underlining the strong adaptive capacity of *S.*
546 *aureus* to withstand the multifactorial challenges imposed by human serum. While serum is acellular
547 and does not reflect the breadth of host-pathogen interactions during bloodstream infections, serum
548 can be an informative proxy for understanding how invading bacteria survive in blood. The key
549 staphylococcal pathways identified here could be further dissected, to explore staphylococcal
550 adaptive responses to identify prospective bacterial (and host) targets for new therapeutic approaches.
551

552 **Limitations of the study**

553 The integrative analysis performed here was highly sensitive and detected subtle patterns linking
554 different omic datasets. However, the metabolic flexibility and functional redundancy within key
555 bacterial pathways - particularly central carbon metabolism and iron acquisition – are likely not
556 limited to individual contributions of specific genes, thus making genes contributing to these
557 pathways difficult to confirm experimentally using single isogenic mutants. Furthermore, the
558 individual contributions of metabolites such as citrate, an intermediate of the TCA cycle, can repress
559 the activity of the transcriptional activity of genes involved in iron homeostasis (101), underscoring
560 the cross-talks between pathways that could alter single -omic readouts, and thus multi-omics
561 analyses. This study used commercially sourced serum for phenotypic confirmation of the
562 staphylococcal signatures. Whilst such reagent offers more control, such as batch control, the
563 concentrations of carbohydrates, metal ions, and reactive oxygen species are unknown, which may

564 influence the significance of phenotypic outputs. Moreover, the datasets analyzed here were
565 generated using pooled human sera (Lifeblood, Melbourne, Australia), whilst our phenotypic
566 confirmation experiments were conducted using commercially sourced and batch-controlled human
567 sera (Sigma Aldrich). The difference in serum processing may explain the discrepant phenotypes
568 obtained for the siderophore-independent *isd* genes involved in iron-scavenging from heme between
569 our current study and the study that generated the datasets (18). Whilst RPMI, closely mimicking the
570 nutrient-limited of the milieu encountered by *S. aureus* during host infection (102), was used as the
571 comparator to serum in our studies ((18) and present study), bacterial omics analyses generated from
572 exposure to alternative media, such as the Human Like Plasma Media (HPLM) (103), enriched in
573 host-like metabolites, could refine the staphylococcal signatures in future analyses.
574
575 **METHODS**
576
577 ***S. aureus* genome and pangenome analyses**
578 The complete genomes of five clinical *S. aureus* strains, BPH2760, BPH2819, BPH2900, BPH2947,
579 BPH2986 (18), and of the strain USA300 JE2 were downloaded from the NCBI database
580 (https://www.ncbi.nlm.nih.gov/bioproject/PRJEB29881/, https://www.ncbi.nlm.nih.
581 gov/bioproject/PRJNA381486).
582 Genomic analysis was conducted using Bohra v2.3.6 (https://github.com/MDU-PHL/bohra). Bohra
583 provided information such as Single Nucleotide Polymorphisms (SNPs), phylogeny, multi-locus
584 sequence typing (MLST), resistome, virulome, and Pan-genome. We used Phandango to visualize the
585 pangenome profiles (https://jameshadfield.github.io/phandango/#/).
586 The AureoWiki database (24) was used to annotate *S. aureus* genes/proteins and to define orthologous
587 relationships, through a reciprocal best hit (RBH) search using MMseqs2 with default parameters
588 (https://github.com/soedinglab/MMseqs2) between the five studied genomes (FAA format) and the

589 *S. aureus* reference genome and proteome (USA300_FPR3757_NCBI_2017 and
590 USA300_FPR3757_NCBI_UniProt_2013).
591
592 **Confirmation of *S. aureus* transposon mutants' genome sequence**
593 We used *S. aureus* transposon mutants of signature genes identified by our analytical pipeline, to
594 verify their fitness in serum. These mutants were selected from the Nebraska transposon library
595 (NTL), including NE275, NE400, NE547, NE665, NE1102, NE1343, and NE1767 (104). The
596 mutants are expected to contain a precise and non-polar transposon insertions, without additional
597 mutations. All mutants were genome sequenced on the Oxford Nanopore platform using Min114 flow
598 cells. Base calling, demultiplexing, and adapter removal were performed in real-time using
599 MinKNOW. Mutant NE1102 was sequenced on a GridION and processed using Guppy. Remaining
600 mutants were sequenced on a MinION and processed using Dorado. FASTQ reads were assembled
601 using Trycycler version 0.5.3 (105). The assembled genomes were compared to the cognate wild-
602 type reference genome using the Mauve whole-genome aligner plugin tool in the Geneious Prime
603 (version 2022.2.2) (106).
604
605 **Serum treatment**
606 We used batch-controlled human serum (Male AB plasma, Sigma Aldrich) to reduce variations
607 arising from different donors. Human serum was clarified from lipids by centrifugation at 3,000 x g
608 during 5 min at 4°C. We further analyzed the protein content of clarified serum (**Figure S9**). Human
609 serum samples (pre (untreated, U) and post (treated, T) centrifugation 5 min at 3000 x g) were diluted
610 1:50 in sterile PBS, then boiled 5 minutes with 5mM DTT in 1x protein loading buffer. Equivalent
611 amounts of proteins were loaded on a Bolt 4%-12% Bis-Tris SDS PAGE gel and separated using with
612 MOPS-SDS running buffer (ThermoFisher, USA) at 100 volts for 1h. The gel was stained with
613 Coomassie blue overnight, destained and imaged using a GE Amersham Imager 800 (GE Life
614 Sciences, UK).

615

616 ***S. aureus* fitness in serum**

617 Overnight cultures of *S. aureus* JE2 (WT), and NTL mutants of *gapdhB*, *sucA*, *htsA*, *sirA*, *sstD*, *isdB*
618 and *perR* were grown from single colonies in 10 ml Brain Heart Infusion media (BHI, BD BACTO™)
619 at 37 °C with orbital shaking. Overnight cultures were centrifuged for 5 min at 5,000 x g, and pellets
620 were washed twice with sterile PBS. The cells were then standardized to an OD 600 nm = 0.5 (0.5
621 UOD) in RPMI (Gibco™). Bacteria equivalent to 0.01 UOD were inoculated in 180 µL of BHI, RPMI
622 or 50% serum (diluted in RPMI) in a clear 96-well plate (Costar), in triplicate to a final volume of
623 200 µL. Plates were incubated at 37°C in ClariostarPLUS microplate reader (BMG Labtech) and
624 bacterial growth was measured every 10 min for 20 h at 600 nm.

625

626 **Phenotypic analysis of *S. aureus* carbohydrate metabolism**

627 Phenotypic profiling was performed using the Biolog Phenotype MicroArray™ (PM) system with
628 PM1 and PM2 plates (Biolog Inc., Hayward, CA, USA), to determine the *S. aureus* fitness in presence
629 of 190 distinct carbon sources. Overnight *S. aureus* cultures were grown in BHI at 37 °C with
630 shaking. Bacterial suspensions were prepared according to the manufacturer's protocol for Gram-
631 positive organisms. The inocula of *gapdhB*, *sucA* and parental WT strain were loaded into PM1 and
632 PM2 plates and incubated at 37 °C for 24 hours in the Biolog Odin™ system, which enables the
633 simultaneous monitoring of growth and respiration (by redox dye reduction). Metabolic activity was
634 assessed by measuring the reduction of tetrazolium-based redox dyes, which serve as indicators of
635 electron transport chain activity in response to specific carbon sources. Dye reduction results in the
636 formation of purple formazan, with absorbance recorded every 20 minutes at 590 nm. The area under
637 the curve (AUC) for each well was calculated to quantify metabolic activity, enabling comparative
638 analysis of carbon source utilization across conditions or strains.

639

640 **Quantification of Staphyloxanthin**

641 Overnight cultures of *S. aureus* JE2 (WT), and NTL mutants of *perR* and *crtM* were grown from
642 single colonies in 25 ml BHI, at 37 °C with orbital shaking. The cultures were standardized to an OD
643 600 nm = 25. These were then centrifuged for 15 min at 5,000 x g, and pellets were washed twice
644 with sterile PBS. Bacteria were incubated in 700 µL of RPMI or in 50% serum (diluted in RPMI) at
645 37 °C with orbital shaking for 5 h. The bacteria were then centrifuged for 5 min at 5,000 x g, and the
646 supernatant was discarded. The pellets were resuspended in 450 µL of methanol, transferred in 1.5
647 ml tubes and incubated at 55 °C for 15 min with shaking. Tubes were centrifuged for 2 min at 13,000
648 RPM, at room temperature. The 100 µL of supernatant from each tube was added to a clear 96-well
649 plate (Costar) in triplicate and extracted staphyloxanthin was quantified at 450 nm using a
650 ClariostarPLUS microplate reader (BMG Labtech). Staphyloxanthin production was calculated by
651 subtracting each data point from the mean absorbance of *crtM* to normalize different condition
652 backgrounds (RPMI and Serum). Replicates were generated from 4 different cultures for each strain,
653 assessed in technical triplicate across two distinct commercial serum batches.
654
655 **Principal component analysis**
656 Principal Component Analysis (PCA) was independently performed on each omics dataset—
657 transcriptomics, proteomics, GC-MS metabolomics, and LC-MS metabolomics—to explore global
658 data structure and identify the primary sources of variation between serum- and RPMI-exposed
659 samples. PCA was conducted using the *pca()* function from the mixOmics package (v6.24.0) in R
660 (v4.2.3), with data scaled to unit variance. The optimal number of components was determined using
661 the tune.pca() function, which indicated that the first three components captured approximately 50%
662 of the total variance across datasets.
663
664 **Multi-omics data integration**
665 We implemented the MixOmics data analytic pipeline known as Multiblock (s)PLS-DA or DIABLO,
666 a multivariate statistical method for classifying and separating different categorical classes (19, 20).

667 This supervised multi-omics integrative method adds sparsity to the model, improving result
668 interpretability by selecting the most relevant variables and setting others' coefficients to zero.
669 DIABLO treats each omics dataset as a separate “block” and identifies co-variation patterns across
670 these blocks, to determine interactions between, and changes by, biological molecules under various
671 conditions. The DIABLO model was designed with a selected design matrix weight of 0.5 to balance
672 discrimination between conditions and correlation across omics layers, ensuring that feature selection
673 prioritized both inter-omics agreement and RPMI-Serum separation. An initial model trained with
674 five components revealed that the first component alone was sufficient to clearly discriminate
675 between serum and RPMI conditions. To assess model robustness and guide component selection,
676 we performed leave-one-out (LOO) cross-validation, which confirmed that a single component
677 provided perfect classification performance. To optimize feature selection for each omics layer, we
678 performed parameter tuning using the tune.block.splsda function. A grid of candidate values for the
679 number of features to retain per block was defined: 20–100 (step size 20) for transcriptomics and
680 proteomics, and 10–100 (step size 10) for both metabolomics datasets (GC-MS and LC-MS). The
681 model was tuned using 5-fold cross-validation repeated 10 times and centroid distance as the
682 classification metric. The number of features retained per block was: 20 for transcriptomics, 20 for
683 proteomics, 10 for GC-MS, and 10 for LC-MS, totaling 60 features. Using these parameters, the final
684 DIABLO model was built using block.splsda function with one component (as determined during
685 component tuning)(19, 20).
686
687 **Enrichment analysis**
688 To identify staphylococcal pathways prominently represented following exposure to serum, feature
689 lists derived from all omics data underwent pathway enrichment analysis, using over-representation
690 analysis (ORA) and Gene Set Enrichment Analysis (GSEA). Pathway enrichment analysis was
691 performed with package clusterProfiler v4.6.2. The obtained feature lists were mapped to the
692 associated biological annotation terms (e.g. GO terms or KEGG pathways) and statistical tests for

693 enrichment probability (enrichment P-value) were calculated to obtain the enrichment of the feature
694 sets. In ORA, the preselected features were filtered by a criterion of log2FC > 1 and p-value < 0.05.
695 For GSEA, all features were ranked based on their log2FC values, meaning features with the largest
696 positive and negative expression changes are positioned at opposite ends of the ranked list, while
697 those with smaller or no changes are located near the middle.
698
699 **Network analysis**
700 The biological relationships among the list of enriched pathways were identified by selecting the
701 significant pathways with p.adjust < 0.05 (except for metabolomic datasets; p-value < 0.05). Further
702 network analysis, using pairwise_termsim function in the enrichplot package in R, calculated the
703 pairwise similarity of the enriched terms using Jaccard's similarity coefficient or the similarity of
704 gene subsets sharing between pathways. Conversion to enrichment map to dataframes provided
705 similarity scores and number of strains sharing individual enriched pathways, represented as node
706 and edge, respectively, for networks' visualization.
707
708 **Data availability**
709 All codes are available on GitHub (https://github.com/warasinee/Multiomics_Analyses_2024).
710 Oxford Nanopore reads of all strains and mutants generated are deposited in NCBI SRA (BioProject
711 ID PRJNA1284587).
712
713 **Acknowledgements**
714 This research was supported by the Development and Promotion of Science and Technology Talents
715 Project (DPST) from the Thai Government (WM), the National Health and Medical Research Council
716 of Australia to BPH (GNT1196103), TPS (GNT1194325), AH, SGG, RG (GNT2018880).
717
718 **References**

1. Howden BP, Giulieri SG, Wong Fok Lung T, Baines SL, Sharkey LK, Lee JYH, et al. Staphylococcus aureus host interactions and adaptation. Nat Rev Microbiol. 2023;21(6):380-95.
2. Räz AK, Andreoni F, Boumasmoud M, Bergada-Pijuan J, Schweizer TA, Mairpady Shambat S, et al. Limited Adaptation of Staphylococcus aureus during Transition from Colonization to Invasive Infection. Microbiol Spectr. 2023;11(4):e0259021.
3. Murray CJ, Ikuta KS, Sharara F, Swetschinski L, Aguilar GR, Gray A, et al. Global burden of bacterial antimicrobial resistance in 2019: a systematic analysis. The lancet. 2022;399(10325):629-55.
4. Guerra FE, Borgogna TR, Patel DM, Sward EW, Voyich JM. Epic Immune Battles of History: Neutrophils vs. Staphylococcus aureus. Front Cell Infect Microbiol. 2017;7:286.
5. Hornef MW, Wick MJ, Rhen M, Normark S. Bacterial strategies for overcoming host innate and adaptive immune responses. Nat Immunol. 2002;3(11):1033-40.
6. Mathew J, Sankar P, Varacallo M. Physiology, Blood Plasma. StatPearls. Treasure Island (FL): StatPearls Publishing
Copyright © 2023, StatPearls Publishing LLC.; 2023.
7. Kuehl R, Morata L, Meylan S, Mensa J, Soriano A. When antibiotics fail: a clinical and microbiological perspective on antibiotic tolerance and persistence of Staphylococcus aureus. J Antimicrob Chemother. 2020;75(5):1071-86.
8. Lopatkin AJ, Stokes JM, Zheng EJ, Yang JH, Takahashi MK, You L, et al. Bacterial metabolic state more accurately predicts antibiotic lethality than growth rate. Nat Microbiol. 2019;4(12):2109-17.
9. Price EE, Boyd JM. Genetic Regulation of Metal Ion Homeostasis in Staphylococcus aureus. Trends Microbiol. 2020;28(10):821-31.
10. Kwiecinski JM, Horswill AR. Staphylococcus aureus bloodstream infections: pathogenesis and regulatory mechanisms. Curr Opin Microbiol. 2020;53:51-60.
11. Bear A, Locke T, Rowland-Jones S, Pecetta S, Bagnoli F, Darton TC. The immune evasion roles of Staphylococcus aureus protein A and impact on vaccine development. Front Cell Infect Microbiol. 2023;13:1242702.
12. de Jong NWM, van Kessel KPM, van Strijp JAG. Immune Evasion by Staphylococcus aureus. Microbiol Spectr. 2019;7(2).
13. Paiva TO, Geoghegan JA, Dufrêne YF. High-force catch bonds between the Staphylococcus aureus surface protein SdrE and complement regulator factor H drive immune evasion. Commun Biol. 2023;6(1):302.
14. Joo HS, Otto M. Mechanisms of resistance to antimicrobial peptides in staphylococci. Biochim Biophys Acta. 2015;1848(11 Pt B):3055-61.
15. Ledger EVK, Mesnage S, Edwards AM. Human serum triggers antibiotic tolerance in Staphylococcus aureus. Nat Commun. 2022;13(1):2041.
16. Murdoch CC, Skaar EP. Nutritional immunity: the battle for nutrient metals at the host-pathogen interface. Nat Rev Microbiol. 2022;20(11):657-70.
17. Cassat JE, Skaar EP. Metal ion acquisition in Staphylococcus aureus: overcoming nutritional immunity. Semin Immunopathol. 2012;34(2):215-35.
18. Mu A, Klare WP, Baines SL, Ignatius Pang CN, Guérillot R, Harbison-Price N, et al. Integrative omics identifies conserved and pathogen-specific responses of sepsis-causing bacteria. Nat Commun. 2023;14(1):1530.
19. Rohart F, Gautier B, Singh A, KA LC. mixOmics: An R package for 'omics feature selection and multiple data integration. PLoS Comput Biol. 2017;13(11):e1005752.
20. Singh A, Shannon CP, Gautier B, Rohart F, Vacher M, Tebbutt SJ, et al. DIABLO: an integrative approach for identifying key molecular drivers from multi-omics assays. Bioinformatics. 2019;35(17):3055-62.
21. González I, Cao KA, Davis MJ, Déjean S. Visualising associations between paired 'omics' data sets. BioData Min. 2012;5(1):19.

770 22. Cox M, Nelson D. Lehninger Principles of Biochemistry. 5 ed: W. H. Freeman and
771 Company; 2008.
772 23. Simon GM, Cravatt BF. Activity-based proteomics of enzyme superfamilies: serine
773 hydrolases as a case study. J Biol Chem. 2010;285(15):11051-5.
774 24. Fuchs S, Mehlan H, Bernhardt J, Hennig A, Michalik S, Surmann K, et al. AureoWiki‐The
775 repository of the Staphylococcus aureus research and annotation community. Int J Med Microbiol.
776 2018;308(6):558-68.
777 25. Ghssein G, Brutesco C, Ouerdane L, Fojcik C, Izaute A, Wang S, et al. Biosynthesis of a
778 broad-spectrum nicotianamine-like metallophore in Staphylococcus aureus. Science.
779 2016;352(6289):1105-9.
780 26. Grim KP, San Francisco B, Radin JN, Brazel EB, Kelliher JL, Párraga Solórzano PK, et al.
781 The Metallophore Staphylopine Enables Staphylococcus aureus To Compete with the Host for Zinc
782 and Overcome Nutritional Immunity. mBio. 2017;8(5).
783 27. Remy L, Carrière M, Derré-Bobillot A, Martini C, Sanguinetti M, Borezée-Durant E. The
784 Staphylococcus aureus Opp1 ABC transporter imports nickel and cobalt in zinc-depleted conditions
785 and contributes to virulence. Mol Microbiol. 2013;87(4):730-43.
786 28. Jongerius I, Garcia BL, Geisbrecht BV, van Strijp JAG, Rooijakkers SHM. Convertase
787 inhibitory properties of Staphylococcal extracellular complement-binding protein. J Biol Chem.
788 2010;285(20):14973-9.
789 29. Purves J, Cockayne A, Moody PC, Morrissey JA. Comparison of the regulation, metabolic
790 functions, and roles in virulence of the glyceraldehyde-3-phosphate dehydrogenase homologues
791 gapA and gapB in Staphylococcus aureus. Infect Immun. 2010;78(12):5223-32.
792 30. Jorge AM, Schneider J, Unsleber S, Göhring N, Mayer C, Peschel A. Utilization of
793 glycerophosphodiesters by Staphylococcus aureus. Mol Microbiol. 2017;103(2):229-41.
794 31. Gustafson J, Strässle A, Hächler H, Kayser FH, Berger-Bächi B. The femC locus of
795 Staphylococcus aureus required for methicillin resistance includes the glutamine synthetase operon.
796 J Bacteriol. 1994;176(5):1460-7.
797 32. Wolff DW, Deng Z, Bianchi-Smiraglia A, Foley CE, Han Z, Wang X, et al. Phosphorylation
798 of guanosine monophosphate reductase triggers a GTP-dependent switch from pro- to anti-
799 oncogenic function of EPHA4. Cell Chem Biol. 2022;29(6):970-84.e6.
800 33. Beasley FC, Marolda CL, Cheung J, Buac S, Heinrichs DE. Staphylococcus aureus
801 transporters Hts, Sir, and Sst capture iron liberated from human transferrin by Staphyloferrin A,
802 Staphyloferrin B, and catecholamine stress hormones, respectively, and contribute to virulence.
803 Infect Immun. 2011;79(6):2345-55.
804 34. Mathelié-Guinlet M, Viela F, Alfeo MJ, Pietrocola G, Speziale P, Dufrêne YF. Single-
805 Molecule Analysis Demonstrates Stress-Enhanced Binding between Staphylococcus aureus Surface
806 Protein IsdB and Host Cell Integrins. Nano Lett. 2020;20(12):8919-25.
807 35. Alfeo MJ, Pagotto A, Barbieri G, Foster TJ, Vanhoorelbeke K, De Filippis V, et al.
808 Staphylococcus aureus iron-regulated surface determinant B (IsdB) protein interacts with von
809 Willebrand factor and promotes adherence to endothelial cells. Sci Rep. 2021;11(1):22799.
810 36. Burman JD, Leung E, Atkins KL, O'Seaghdha MN, Lango L, Bernadó P, et al. Interaction of
811 human complement with Sbi, a staphylococcal immunoglobulin-binding protein: indications of a
812 novel mechanism of complement evasion by Staphylococcus aureus. J Biol Chem.
813 2008;283(25):17579-93.
814 37. Overton TW, Justino MC, Li Y, Baptista JM, Melo AM, Cole JA, et al. Widespread
815 distribution in pathogenic bacteria of di-iron proteins that repair oxidative and nitrosative damage to
816 iron-sulfur centers. J Bacteriol. 2008;190(6):2004-13.
817 38. Brunskill EW, de Jonge BLM, Bayles KW. The Staphylococcus aureus scdA gene: a novel
818 locus that affects cell division and morphogenesis. Microbiology (Reading). 1997;143 (Pt 9):2877-
819 82.

820 39. Zhang W, Zhang M, Gao C, Zhang Y, Ge Y, Guo S, et al. Coupling between d-3-
821 phosphoglycerate dehydrogenase and d-2-hydroxyglutarate dehydrogenase drives bacterial l-serine
822 synthesis. Proc Natl Acad Sci U S A. 2017;114(36):E7574-e82.
823 40. Rack JG, Morra R, Barkauskaite E, Kraehenbuehl R, Ariza A, Qu Y, et al. Identification of
824 a Class of Protein ADP-Ribosylating Sirtuins in Microbial Pathogens. Mol Cell. 2015;59(2):309-20.
825 41. Arragain S, Handelman SK, Forouhar F, Wei FY, Tomizawa K, Hunt JF, et al. Identification
826 of eukaryotic and prokaryotic methylthiotransferase for biosynthesis of 2-methylthio-N6-
827 threonylcarbamoyladenosine in tRNA. J Biol Chem. 2010;285(37):28425-33.
828 42. Murphey WH, Rosenblum ED. MANNITOL CATABOLISM BY STAPHYLOCOCCUS
829 AUREUS. Arch Biochem Biophys. 1964;107:292-7.
830 43. Ji CJ, Kim JH, Won YB, Lee YE, Choi TW, Ju SY, et al. Staphylococcus aureus PerR Is a
831 Hypersensitive Hydrogen Peroxide Sensor using Iron-mediated Histidine Oxidation. J Biol Chem.
832 2015;290(33):20374-86.
833 44. Leibig M, Liebeke M, Mader D, Lalk M, Peschel A, Götz F. Pyruvate formate lyase acts as
834 a formate supplier for metabolic processes during anaerobiosis in Staphylococcus aureus. J
835 Bacteriol. 2011;193(4):952-62.
836 45. Bertrand BP, Heim CE, West SC, Chaudhari SS, Ali H, Thomas VC, et al. Role of
837 Staphylococcus aureus Formate Metabolism during Prosthetic Joint Infection. Infect Immun.
838 2022;90(11):e0042822.
839 46. Handa N, Terada T, Doi-Katayama Y, Hirota H, Tame JR, Park SY, et al. Crystal structure
840 of a novel polyisoprenoid-binding protein from Thermus thermophilus HB8. Protein Sci.
841 2005;14(4):1004-10.
842 47. Rack JGM, Palazzo L, Ahel I. (ADP-ribosyl)hydrolases: structure, function, and biology.
843 Genes Dev. 2020;34(5-6):263-84.
844 48. Christgen SL, Becker DF. Role of Proline in Pathogen and Host Interactions. Antioxid
845 Redox Signal. 2019;30(4):683-709.
846 49. Richardson AR, Somerville GA, Sonenshein AL. Regulating the Intersection of Metabolism
847 and Pathogenesis in Gram-positive Bacteria. Microbiol Spectr. 2015;3(3).
848 50. Kim J, Kim GL, Norambuena J, Boyd JM, Parker D. Impact of the pentose phosphate
849 pathway on metabolism and pathogenesis of Staphylococcus aureus. PLoS Pathog.
850 2023;19(7):e1011531.
851 51. Njenga R, Boele J, Öztürk Y, Koch HG. Coping with stress: How bacteria fine-tune protein
852 synthesis and protein transport. J Biol Chem. 2023;299(9):105163.
853 52. Gibbs MR, Moon KM, Warner BR, Chen M, Bundschuh R, Foster LJ, et al. Functional
854 Analysis of BipA in E. coli Reveals the Natural Plasticity of 50S Subunit Assembly. J Mol Biol.
855 2020;432(19):5259-72.
856 53. Esquilin-Lebron K, Dubrac S, Barras F, Boyd JM. Bacterial Approaches for Assembling
857 Iron-Sulfur Proteins. mBio. 2021;12(6):e0242521.
858 54. Barrault M, Leclair E, Kumeko EK, Jacquet E, Bouloc P. Staphylococcal sRNA IsrR
859 downregulates methylthiotransferase MiaB under iron-deficient conditions. Microbiol Spectr.
860 2024;12(10):e0388823.
861 55. Sheldon JR, Marolda CL, Heinrichs DE. TCA cycle activity in Staphylococcus aureus is
862 essential for iron-regulated synthesis of staphyloferrin A, but not staphyloferrin B: the benefit of a
863 second citrate synthase. Mol Microbiol. 2014;92(4):824-39.
864 56. Pishchany G, Sheldon JR, Dickson CF, Alam MT, Read TD, Gell DA, et al. IsdB-dependent
865 hemoglobin binding is required for acquisition of heme by Staphylococcus aureus. J Infect Dis.
866 2014;209(11):1764-72.
867 57. Imlay JA. Cellular defenses against superoxide and hydrogen peroxide. Annu Rev Biochem.
868 2008;77:755-76.
869 58. Toledano MB, Delaunay A, Monceau L, Tacnet F. Microbial H2O2 sensors as archetypical
870 redox signaling modules. Trends Biochem Sci. 2004;29(7):351-7.

871 59. Dubbs JM, Mongkolsuk S. Peroxide-sensing transcriptional regulators in bacteria. J
872 Bacteriol. 2012;194(20):5495-503.
873 60. Horsburgh MJ, Clements MO, Crossley H, Ingham E, Foster SJ. PerR controls oxidative
874 stress resistance and iron storage proteins and is required for virulence in Staphylococcus aureus.
875 Infect Immun. 2001;69(6):3744-54.
876 61. Hines KM, Alvarado G, Chen X, Gatto C, Pokorny A, Alonzo F, 3rd, et al. Lipidomic and
877 Ultrastructural Characterization of the Cell Envelope of Staphylococcus aureus Grown in the
878 Presence of Human Serum. mSphere. 2020;5(3).
879 62. Beasley FC, Cheung J, Heinrichs DE. Mutation of L-2,3-diaminopropionic acid synthase
880 genes blocks staphyloferrin B synthesis in Staphylococcus aureus. BMC Microbiol. 2011;11:199.
881 63. Carvalho SM, de Jong A, Kloosterman TG, Kuipers OP, Saraiva LM. The Staphylococcus
882 aureus α-Acetolactate Synthase ALS Confers Resistance to Nitrosative Stress. Front Microbiol.
883 2017;8:1273.
884 64. Gaupp R, Ledala N, Somerville GA. Staphylococcal response to oxidative stress. Front Cell
885 Infect Microbiol. 2012;2:33.
886 65. Halsey CR, Lei S, Wax JK, Lehman MK, Nuxoll AS, Steinke L, et al. Amino Acid
887 Catabolism in Staphylococcus aureus and the Function of Carbon Catabolite Repression. mBio.
888 2017;8(1).
889 66. Imada A, Nozaki Y, Kawashima F, Yoneda M. Regulation of glucosamine utilization in
890 Staphylococcus aureus and Escherichia coli. J Gen Microbiol. 1977;100(2):329-37.
891 67. Kenny JG, Moran J, Kolar SL, Ulanov A, Li Z, Shaw LN, et al. Mannitol utilisation is
892 required for protection of Staphylococcus aureus from human skin antimicrobial fatty acids. PLoS
893 One. 2013;8(7):e67698.
894 68. Kriegeskorte A, Block D, Drescher M, Windmüller N, Mellmann A, Baum C, et al.
895 Inactivation of thyA in Staphylococcus aureus attenuates virulence and has a strong impact on
896 metabolism and virulence gene expression. mBio. 2014;5(4):e01447-14.
897 69. Nolan AC, Zeden MS, Kviatkovski I, Campbell C, Urwin L, Corrigan RM, et al. Purine
898 Nucleosides Interfere with c-di-AMP Levels and Act as Adjuvants To Re-Sensitize MRSA To β-
899 Lactam Antibiotics. mBio. 2023;14(1):e0247822.
900 70. O'Connor MJ, Bartler AV, Ho KC, Zhang K, Casas Fuentes RJ, Melnick BA, et al.
901 Understanding Staphylococcus aureus in hyperglycaemia: A review of virulence factor and
902 metabolic adaptations. Wound Repair Regen. 2024;32(5):661-70.
903 71. Parsons JB, Rock CO. Bacterial lipids: metabolism and membrane homeostasis. Prog Lipid
904 Res. 2013;52(3):249-76.
905 72. Potter AD, Butrico CE, Ford CA, Curry JM, Trenary IA, Tummarakota SS, et al. Host
906 nutrient milieu drives an essential role for aspartate biosynthesis during invasive Staphylococcus
907 aureus infection. Proc Natl Acad Sci U S A. 2020;117(22):12394-401.
908 73. Qi Z, Sun N, Liu C. Glyoxylate cycle maintains the metabolic homeostasis of Pseudomonas
909 aeruginosa in viable but nonculturable state induced by chlorine stress. Microbiol Res.
910 2023;270:127341.
911 74. Sachla AJ, Helmann JD. A bacterial checkpoint protein for ribosome assembly moonlights
912 as an essential metabolite-proofreading enzyme. Nat Commun. 2019;10(1):1526.
913 75. Seo KS, Park N, Rutter JK, Park Y, Baker CL, Thornton JA, et al. Role of Glucose-6-
914 Phosphate in Metabolic Adaptation of Staphylococcus aureus in Diabetes. Microbiol Spectr.
915 2021;9(2):e0085721.
916 76. Clauditz A, Resch A, Wieland KP, Peschel A, Götz F. Staphyloxanthin plays a role in the
917 fitness of Staphylococcus aureus and its ability to cope with oxidative stress. Infect Immun.
918 2006;74(8):4950-3.
919 77. Chang W, Small DA, Toghrol F, Bentley WE. Global transcriptome analysis of
920 Staphylococcus aureus response to hydrogen peroxide. J Bacteriol. 2006;188(4):1648-59.
921 78. Cheung GYC, Bae JS, Otto M. Pathogenicity and virulence of Staphylococcus aureus.
922 Virulence. 2021;12(1):547-69.

923 79. Soe YM, Bedoui S, Stinear TP, Hachani A. Intracellular Staphylococcus aureus and host
924 cell death pathways. Cell Microbiol. 2021;23(5):e13317.
925 80. Ledala N, Zhang B, Seravalli J, Powers R, Somerville GA. Influence of iron and aeration on
926 Staphylococcus aureus growth, metabolism, and transcription. J Bacteriol. 2014;196(12):2178-89.
927 81. Fouché A, Zinovyev A. Omics data integration in computational biology viewed through the
928 prism of machine learning paradigms. Front Bioinform. 2023;3:1191961.
929 82. Maghsoudi Z, Nguyen H, Tavakkoli A, Nguyen T. A comprehensive survey of the
930 approaches for pathway analysis using multi-omics data integration. Brief Bioinform. 2022;23(6).
931 83. Vahabi N, Michailidis G. Unsupervised Multi-Omics Data Integration Methods: A
932 Comprehensive Review. Front Genet. 2022;13:854752.
933 84. Campbell C, Fingleton C, Zeden MS, Bueno E, Gallagher LA, Shinde D, et al.
934 Accumulation of Succinyl Coenzyme A Perturbs the Methicillin-Resistant Staphylococcus aureus
935 (MRSA) Succinylome and Is Associated with Increased Susceptibility to Beta-Lactam Antibiotics.
936 mBio. 2021;12(3):e0053021.
937 85. Harper L, Balasubramanian D, Ohneck EA, Sause WE, Chapman J, Mejia-Sosa B, et al.
938 Staphylococcus aureus Responds to the Central Metabolite Pyruvate To Regulate Virulence. mBio.
939 2018;9(1).
940 86. Tomlinson KL, Riquelme SA. Host-bacteria metabolic crosstalk drives S. aureus biofilm.
941 Microb Cell. 2021;8(5):106-7.
942 87. Tomlinson KL, Lung TWF, Dach F, Annavajhala MK, Gabryszewski SJ, Groves RA, et al.
943 Staphylococcus aureus induces an itaconate-dominated immunometabolic response that drives
944 biofilm formation. Nat Commun. 2021;12(1):1399.
945 88. Passalacqua KD, Charbonneau ME, O'Riordan MXD. Bacterial Metabolism Shapes the
946 Host-Pathogen Interface. Microbiol Spectr. 2016;4(3).
947 89. Zhao R, Xu L, Chen J, Yang Y, Guo X, Dai M, et al. Itaconate induces tolerance of
948 Staphylococcus aureus to aminoglycoside antibiotics. Front Microbiol. 2024;15:1450085.
949 90. Ramond E, Gesbert G, Rigard M, Dairou J, Dupuis M, Dubail I, et al. Glutamate utilization
950 couples oxidative stress defense and the tricarboxylic acid cycle in Francisella phagosomal escape.
951 PLoS Pathog. 2014;10(1):e1003893.
952 91. Tavares AF, Teixeira M, Romão CC, Seixas JD, Nobre LS, Saraiva LM. Reactive oxygen
953 species mediate bactericidal killing elicited by carbon monoxide-releasing molecules. J Biol Chem.
954 2011;286(30):26708-17.
955 92. Yee R, Cui P, Shi W, Feng J, Zhang Y. Genetic Screen Reveals the Role of Purine
956 Metabolism in Staphylococcus aureus Persistence to Rifampicin. Antibiotics (Basel).
957 2015;4(4):627-42.
958 93. Yee R, Feng J, Wang J, Chen J, Zhang Y. Identification of Genes Regulating Cell Death in
959 Staphylococcus aureus. Front Microbiol. 2019;10:2199.
960 94. Malachowa N, Whitney AR, Kobayashi SD, Sturdevant DE, Kennedy AD, Braughton KR,
961 et al. Global changes in Staphylococcus aureus gene expression in human blood. PLoS One.
962 2011;6(4):e18617.
963 95. Haupt K, Reuter M, van den Elsen J, Burman J, Hälbich S, Richter J, et al. The
964 Staphylococcus aureus protein Sbi acts as a complement inhibitor and forms a tripartite complex
965 with host complement Factor H and C3b. PLoS Pathog. 2008;4(12):e1000250.
966 96. Yan J, Han D, Liu C, Gao Y, Li D, Liu Y, et al. Staphylococcus aureus VraX specifically
967 inhibits the classical pathway of complement by binding to C1q. Mol Immunol. 2017;88:38-44.
968 97. Spaan AN, Vrieling M, Wallet P, Badiou C, Reyes-Robles T, Ohneck EA, et al. The
969 staphylococcal toxins γ-haemolysin AB and CB differentially target phagocytes by employing
970 specific chemokine receptors. Nat Commun. 2014;5:5438.
971 98. Zhao Y, van Kessel KPM, de Haas CJC, Rogers MRC, van Strijp JAG, Haas PA.
972 Staphylococcal superantigen-like protein 13 activates neutrophils via formyl peptide receptor 2.
973 Cell Microbiol. 2018;20(11):e12941.

99. Higgins J, Loughman A, van Kessel KP, van Strijp JA, Foster TJ. Clumping factor A of Staphylococcus aureus inhibits phagocytosis by human polymorphonuclear leucocytes. FEMS Microbiol Lett. 2006;258(2):290-6.
100. Smith EJ, Visai L, Kerrigan SW, Speziale P, Foster TJ. The Sbi protein is a multifunctional immune evasion factor of Staphylococcus aureus. Infect Immun. 2011;79(9):3801-9.
101. Chen F, Zhao Q, Yang Z, Chen R, Pan H, Wang Y, et al. Citrate serves as a signal molecule to modulate carbon metabolism and iron homeostasis in Staphylococcus aureus. PLoS Pathog. 2024;20(7):e1012425.
102. Poudel S, Tsunemoto H, Seif Y, Sastry AV, Szubin R, Xu S, et al. Revealing 29 sets of independently modulated genes in Staphylococcus aureus, their regulators, and role in key physiological response. Proc Natl Acad Sci U S A. 2020;117(29):17228-39.
103. Cascales E. Inside the Chamber of Secrets of the Type III Secretion System. Cell. 2017;168(6):949-51.
104. Fey PD, Endres JL, Yajjala VK, Widhelm TJ, Boissy RJ, Bose JL, et al. A genetic resource for rapid and comprehensive phenotype screening of nonessential Staphylococcus aureus genes. mBio. 2013;4(1):e00537-12.
105. Wick RR, Judd LM, Cerdeira LT, Hawkey J, Méric G, Vezina B, et al. Trycycler: consensus long-read assemblies for bacterial genomes. Genome Biol. 2021;22(1):266.
106. Darling AC, Mau B, Blattner FR, Perna NT. Mauve: multiple alignment of conserved genomic sequence with rearrangements. Genome Res. 2004;14(7):1394-403.